



A Paper-Fiber-Supported 3D SERS Substrate

Yunyun Mu¹ · Xinping Zhang¹

Received: 16 September 2019 / Accepted: 4 December 2019 / Published online: 24 December 2019
© Springer Science+Business Media, LLC, part of Springer Nature 2019

Abstract

Surface-enhanced Raman scattering (SERS) spectroscopy is an effective approach for trace-level detection of molecular substance. Plasmonic metallic nanostructures with high distribution densities and small gap widths are always expected for constructing SERS substrates. We report here a paper-based SERS substrate, where the three-dimensional (3D) network of paper fibers was used as the platform for supporting the gold nanoparticle clusters. Such a 3D arrangement of plasmonic porous clusters supplies high-density hotspots with large total volume and large surface area for the interaction with molecules. Comparison between different papers found that the filter papers commonly available in labs are the best choice. An enhancement factor higher than 10^4 has been achieved in the detection of R6G molecules. The preparation of such SERS substrates is very simple and convenient, implying low-cost, disposable, and environment-friendly SERS techniques. Furthermore, the paper-based flexible SERS substrates can be easily tailored into different shapes and sizes for fitting different applications.

Keywords Paper substrate · Flexibly tailorable SERS substrate · Paper fibers · Three-dimensional network · Gold nanoparticle clusters · Filter papers

Introduction

Surface-enhanced Raman scattering (SERS) spectroscopy is widely applied in the detection of low concentration molecules [1–6] and pesticides [6–9]. As an efficient method for trace detection, SERS supplies selectively enhanced Raman signals with high intensity. Plasmonic local fields, which are generally identified as hotspots, enable strong interaction between optical electric fields and environmental molecules. Localized surface plasmon resonance (LSPR) spectrum of Au, Ag, and Cu nanostructures may cover the whole visible and near-infrared band [10–15], which is controllable through designing the size [16, 17], the shape [18, 19], and the combination of different materials of the structures [20, 21]. Therefore, nanostructured substrates with these metals have been widely employed in SERS device design. Although a large variety of SERS substrates have been demonstrated using different metal nanostructures, there is still large space to optimize the designs to satisfy the ever-

increasing requirements on the performance and various applications of the SERS detection techniques. Conventionally, SERS substrates are produced by metallic nanostructures on glass substrates [22–24] or silicon wafers [25–28]. However, three-dimensional (3D) structures are more advantageous in SERS applications, which enlarge both the interaction volumes and total interaction surface areas between the localized field and the molecules to be detected. The complexity of the fabrication procedures, relatively large thickness and low-flexibility of the substrates, and high cost of fabrication equipment and materials limit the practical application of these SERS devices. Novel methods are always being developed for the fabrication of efficient SERS substrates, such as electrostatic spinning, which provides a simple and templateless method for the preparation of 3D SERS substrates based on polymer fibers [29–31]. On this basis, various 3D polymer nano-fiber-based metallic nanostructures have been demonstrated for high-sensitivity sensors using SERS effects [32–35].

In this work, we demonstrate an economical and simple method for fabricating 3D SERS substrates, where the paper fiber network is used as the frame for the plasmonic nanostructures. Chemical synthesized gold nanoparticles coated with tetraoctylammonium bromide are adsorbed to the paper fibers, forming gold nanoparticle clusters and producing high-density hotspots for SERS detection. An enhancement factor

✉ Xinping Zhang
zhangxinping@bjut.edu.cn

¹ Institute of Information Photonics Technology and College of Applied Sciences, Beijing University of Technology, Beijing 100124, China

larger than 10^4 has been achieved. High simplicity, easy fabrication, low costs, thin, and flexible devices with easily tailorable shapes and sizes are the apparent advantages of the present SERS substrate over the conventional designs.

Preparation of the SERS Substrates

Gold nanoparticles (AuNPs) coated with tetraoctylammonium bromide (TOABr) were first synthesized chemically with the detailed preparation recipe included in the experimental section. They are then suspended in acetone with excellent dispersity to prepare the colloidal solution. A concentration of 50 mg/mL for the colloidal solution was found to be an optimized value for the SERS substrate preparation after a series of test experiments. Three kinds of papers that are commonly available in the laboratories or in daily life were employed in the preparation of the SERS substrates, which include the filter papers, printing papers, and envelope papers. These papers have different textures of paper fibers and different thickness of the fibers, so that the sample solutions also wet these paper surfaces differently. A 30- μ L colloidal solution was drop-cast onto the paper surface. Then, the paper substrate was heated at 110°C on a hotplate for 2 min to evaporate the solvent and to finish the metallization process. At such a temperature, the TOABr coating on the AuNPs was not removed. Thus, after being metallized, the papers exhibit different morphological performances. The AuNPs coated on the paper fibers have different sizes and different density distributions.

Figure 1a–c show the SEM images measured on the surface of filter paper, printing paper, and envelope paper, respectively, before they are coated with AuNPs. It needs to be noted that the AuNPs here are all adsorbed with TOABr. 3D textures are clearly observed for the papers, where the paper fibers exhibit slightly different diameters and different networks for different papers. Thus, large surface area can be obtained using such 3D textures. The widths of the paper fibers are slightly different for different papers, which were measured to be in the range of 7–20 μ m.

Figure 1d–f show the SEM images of the metalized paper surface, corresponding to their precursors in Figs. 1a–c, respectively. The colloidal AuNPs are aggregated into large-scale clusters consisting of a large amount of small gold nanoparticles, and they are attached to the paper fibers. As shown in the insets of Fig. 1d–f, each cluster is a porous bulk constituted by closely packed gold nanoparticles with very small sizes and very small gap widths, which supply high-density hotspots with potentially significantly enhanced local field. This is an ideal configuration for ideal SERS substrates. When comparing Fig. 1d with Fig. 1e and f, we may find that for a filter paper the clusters are larger than those for a printing paper; however, they are less homogeneously distributed. If looking at the insets of Fig. 1d–f, we find that the porous structures of the clusters and size of the gold nanoparticles are not much different between the three samples. Therefore, these substrates should in principle supply similar SERS performance.

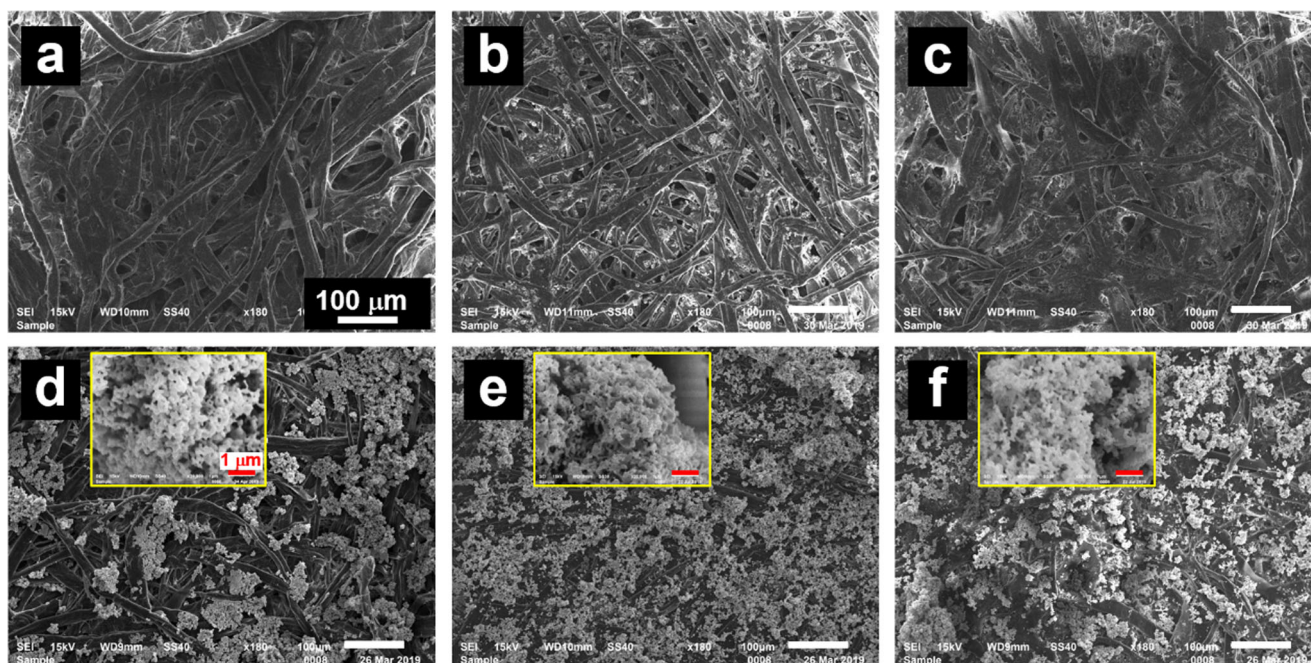


Fig. 1 (a–c) Top view SEM images of the paper fibers measured on the filter paper, printing paper, and envelope paper, respectively. (d–f) SEM images of paper surfaces after being metalized by colloidal gold

nanoparticles, corresponding to the paper substrates in (a–c), respectively. Insets: enlarged views of local areas

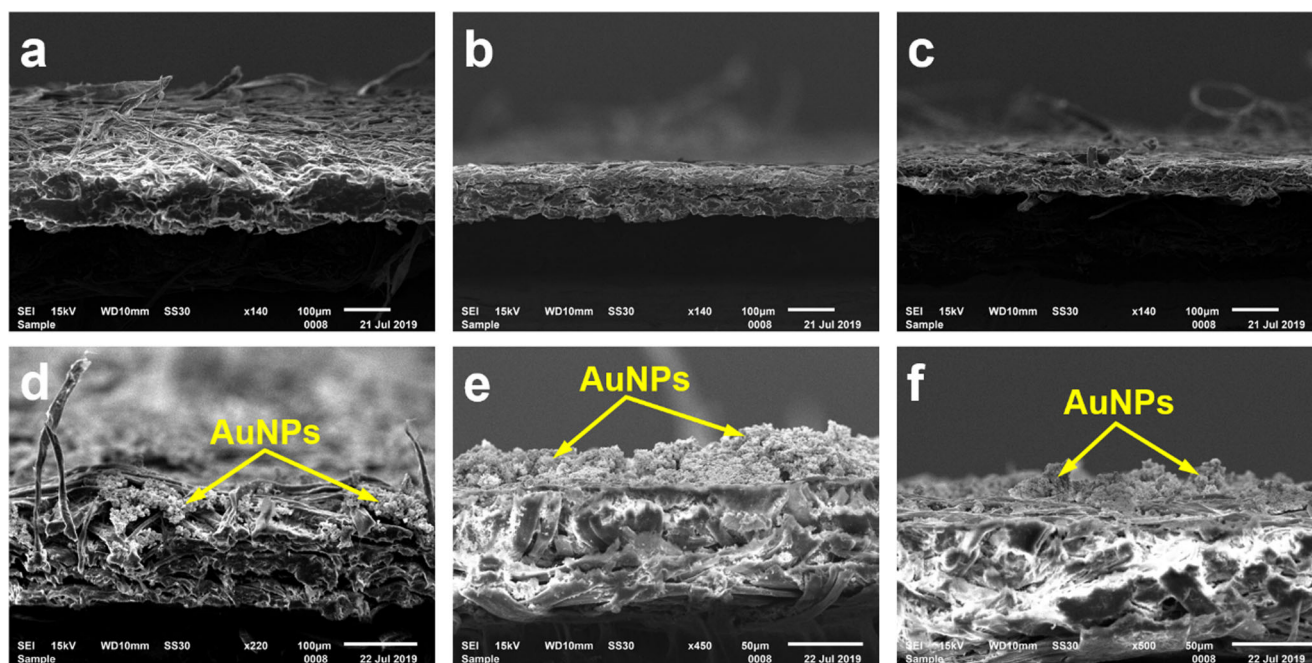


Fig. 2 (a–c) Cross-sectional view SEM images of the paper fibers for the filter paper, printing paper, and envelope paper, respectively. (d–f) Cross-sectional view SEM images of metalized paper substrates in (a–c), respectively

For distinguishing these three types of papers by their microstructural performance, we measured the SEM images of the cross-sectional profiles of them, as shown in Fig. 2a–c for the filter, printing, and envelope papers, respectively. Clearly, the filter paper is the thickest and the envelope paper is the thinnest; moreover, the fibers are much more loosely interlaced in the texture structures of the filter paper than the other two. Furthermore, the filter paper has a roughest surface, as compared with the other two papers. Such a loose and rough-surface configuration favors formation of the 3D distribution of the clusters of gold nanoparticles. This can be confirmed by Fig. 2d for the filter paper, as compared with Fig. 2e and f for the printing and envelope papers. Clearly, the gold nanoparticle clusters are located in the space between the fibers for the filter paper; however, they are mainly piled up on the surface of the printing and envelope papers. Apparently, the SERS substrate based on a piece of filter paper is more reliable and stable, although the three designs exhibit nearly the same SERS enhancement performance, as will be demonstrated in Section 3.2.

For distinguishing these three types of papers, we measured Raman spectra on all of the samples in Fig. 1 using an excitation laser at 785 nm and present the results in the supporting information. Figure 3a shows the Raman spectra measured on the samples in Fig. 2a–c, which are plotted by black, red, and green curves. Clearly, much larger background can be observed with the printing and envelope papers than the filter paper. Similarly, such background difference can also be observed with the samples after being metalized with the gold nanoparticles, as shown in Fig. 3b. The background of the

Raman spectrum is even higher for the printing paper than the envelope paper and that for the filter paper becomes more flat and smooth. Furthermore, some spectral features can be observed with Raman spectra in Fig. 3, as highlighted by downward triangles, which are located at 1106, 1130, and 1385 cm^{-1} . These features resulted from the fluorescent agents that are used for whitening the papers, which are stronger for the printing and envelope papers. However, multiple sharp peaks can be observed with the red curve in Fig. 3b, which can be taken as noise signals. According to the comparison between the three types of papers, the filter paper is the most suitable candidate for the preparation of SERS substrates.

SERS Performance

Detection of R6G Molecules Using TOABr-Coated AuNPs on Paper Fibers

For SERS measurements, a continuous-wave (CW) 785 nm laser with a maximum power of 100 mW was used as the excitation, which was focused into an excitation area of about 2.06 mm^2 . An integration time of 1 s was employed for all measurements. R6G solutions in ethanol with different concentrations were employed, which were drop-cast onto the surface of the paper-based SERS substrates by a volume of 30 μL . SERS measurements were carried out after ethanol evaporates completely.

Figure 4a shows the SERS spectra measured on R6G molecules on the AuNPs-metalized papers, where the black,

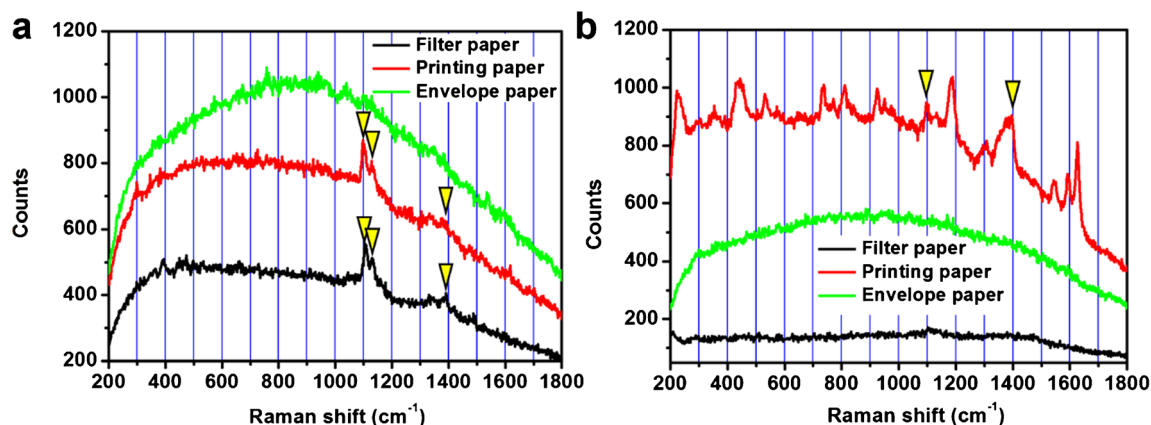


Fig. 3 (a) Raman spectra measured on the filter paper, printing papers, and envelope paper, respectively. (b) Raman spectra measured on different paper substrates as they are coated with AuNPs without molecules for detection

red, and green curves correspond to the measurements using the filter, printing, and envelope papers, respectively. Some typical peaks are enhanced at 1191, 1313, 1433, 1514, 1574, and 1646 cm^{-1} . Locations of these spectral peaks are consistent with the other reported data in literatures [36, 37]. Apparently, large SERS signal can be observed in Fig. 4a for all paper substrates. In particular, the intensity of peak at 1313 cm^{-1} is enhanced most obviously. The concentration of the R6G solution in ethanol for preparation of the sample was 10^{-4} M. Comparing the measurement results using the

three different types of paper substrates, we may observe nearly equal amplitude of the SERS signals; however, nearly flat background can be observed with the filter paper-based SERS substrate. To verify the enhancement effects by the 3D plasmonic AuNPs on paper substrates, we present in Fig. 4b the Raman spectra measured on the R6G molecules drop-casted on pure papers without AuNPs, where we have changed the concentration of the R6G/ethanol solution so that the typical Raman peaks can be resolved from the background. As shown in Fig. 4b, the lowest resolvable

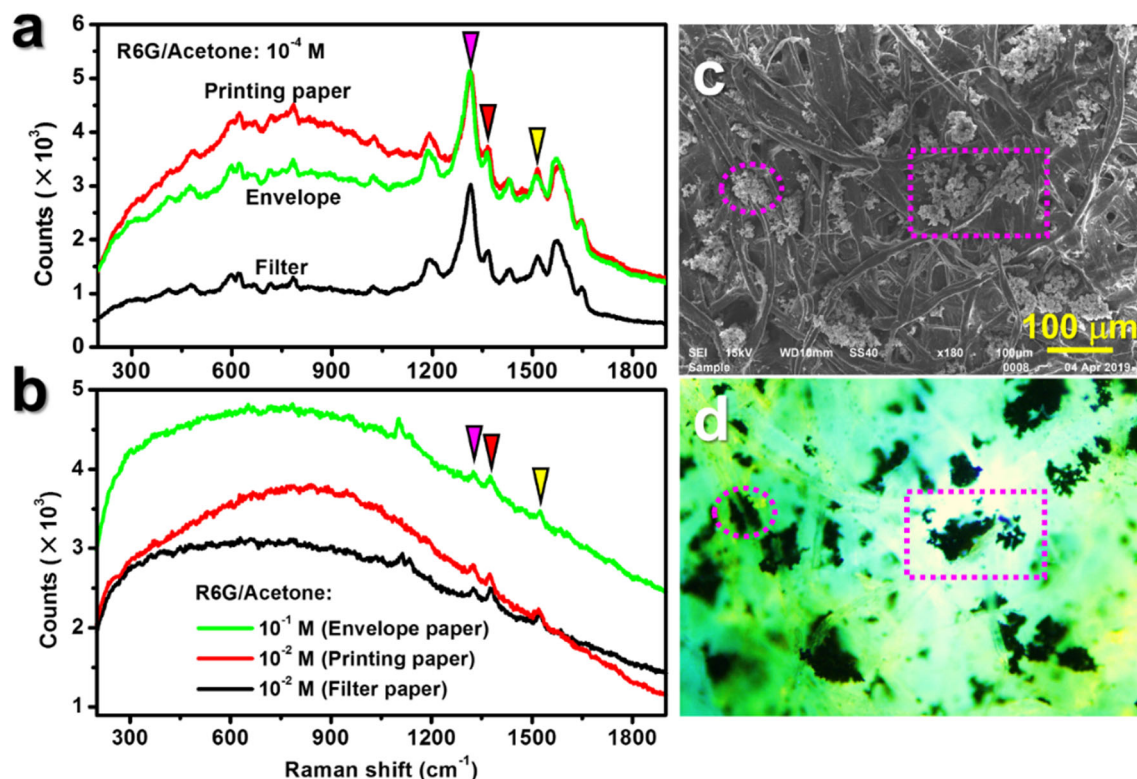


Fig. 4 (a) SERS spectra measured on R6G molecules prepared by drop-casting R6G/ethanol solutions with a concentration of 10^{-4} M onto AuNP-coated filter (black), printing (red), and envelope (black) papers. (b) Raman spectra measured on samples prepared by drop-casting R6G/

ethanol solutions with different concentrations onto pure filter (black), printing (red), and envelope (green) papers without AuNPs coating. (c) SEM image of the AuNP-coated filter paper. (d) Fluorescence optical microscope image measured in the same region as the SEM image in (c)

concentration is 10^{-1} M for the envelope paper and 10^{-2} M for the filter and printing papers. If we evaluate the enhancement factor (EF) roughly by

$$EF = \frac{I_{SERS} \times C_{RS}}{I_{RS} \times C_{SERS}}, \quad (1)$$

where I_{SERS} and I_{RS} are the amplitudes of the SERS and Raman signals, respectively, and the C_{RS} and C_{SERS} are the solution concentrations for the Raman and SERS measurements, respectively, the values of EF can be calculated to be in the range $0.3\text{--}1.68 \times 10^4$. This verifies the excellent SERS effects of AuNPs on the paper substrates. The correspondence between the Raman peaks for evaluating the enhancement factors is indicated by the downward triangles in Fig. 4a and b. Figure 4c shows the SEM image of the AuNPs prepared on the filter paper substrate before being drop-cast with R6G/ethanol solution, whereas Fig. 4d shows the fluorescence optical microscope images measured on the same area as the SEM image after the drop-casting of R6G/ethanol solution. The dashed circle and rectangle highlights the correspondence between the two microscopic images. The R6G molecules can be identified by the yellow-greenish colors, which results from the emission from R6G molecules after being excited by a UV light source. According to Fig. 3d, the R6G molecules are more aggregated in the area around the AuNPs, favoring the enhancement of the interaction between the local plasmonic fields and the R6G molecules.

Enhancement Factor

Comparison with Raman Spectroscopy Based on Pure Paper Substrate

To evaluate the SERS enhancement factor more precisely, we performed a series of experiments using the substrate demonstrated in Fig. 4b and c to measure the SERS spectra on different concentrations of the R6G/ethanol solutions. As shown in Fig. 5, as the concentration of R6G/ethanol solution was reduced from 10^{-3} M to 10^{-6} M, the absolute amplitude (S_A , as defined in Fig. 5) of the SERS signal at 1313 cm^{-1} was reduced from 3285 to 140 counts. However, the signal is still clearly seen with excellent signal-to-noise ratio, implying reliable detection at a concentration of 10^{-6} M. For substrates using pure filter papers without AuNPs coating, reliably resolvable Raman spectral peaks can be observed only when the solution concentration was increased to 10^{-2} M. In the inset of Fig. 5, we compare this Raman spectrum for a concentration of 10^{-2} M (black) with the SERS spectrum for a concentration of 10^{-6} M (blue). The correspondence between the Raman peaks is highlighted by triangles with different colors. Using the definition of the enhancement factor in Eq. (1) and the

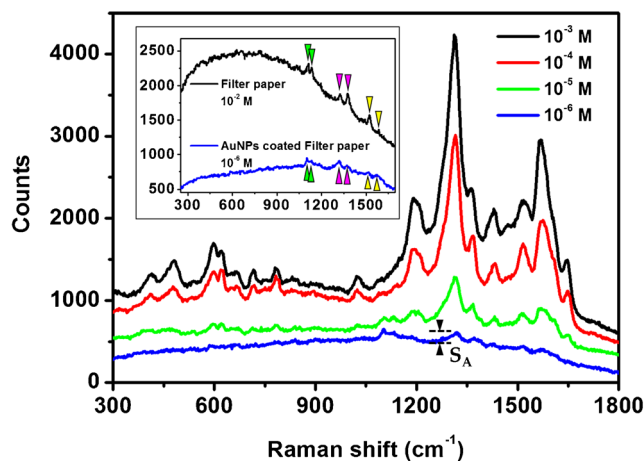


Fig. 5 SERS spectra measured on R6G molecules prepared by drop casting R6G/ethanol solutions with different concentrations onto an AuNP-coated filter paper substrate. Inset: comparison between the Raman spectroscopic measurement on a pure filter paper for R6G/ethanol solution with a concentration of 10^{-2} M and the SERS performance on an AuNP-coated filter paper for a R6G/ethanol solution concentration of 10^{-6} M

absolute signal amplitudes that can be determined by the inset of Fig. 5, we can calculate the enhancement factor at 1313 cm^{-1} to be about $EF = 1.4 \times 10^4$.

Comparison with Raman Spectroscopy Based on Pure Glass Substrate

It is also useful to compare the AuNP-coated paper SERS substrate with the pure glass substrate, where glass substrates are commonly employed in Raman and SERS measurements. We compare the measurement results in Fig. 6a, where the black curve shows the SERS spectrum measured on the sample prepared by R6G/ethanol solution with a concentration of 10^{-6} M and the red was measured on the sample prepared using a concentration of 10^{-2} M on a glass substrate. Using Eq. (1), we may calculate a SERS enhancement factor of $EF = 4.6 \times 10^4$. Thus, the 3D TOABr-coated AuNPs structures supported by fibers of the filter paper substrate render high enhancement factor, as compared with conventional glass substrates. Furthermore, much larger background modulation can be observed with the glass substrate than the filter paper, as indicated by the upward arrow.

For better understanding on the mechanisms for the SERS performance, we also need to consider the rough surface and large total area supplied by the paper fiber network coated with gold nanoparticles. As shown in Fig. 6b, the paper fibers coated with AuNPs have a large spatial modulation in three dimensions, implying enlarged interaction volumes. The modulation depth distributes in a broad range of 0–1180 nm, producing an *rms* value of 295 nm. Such rough surfaces enable enhanced interaction between localized surface plasmons and the target molecules through intensified local field, densified

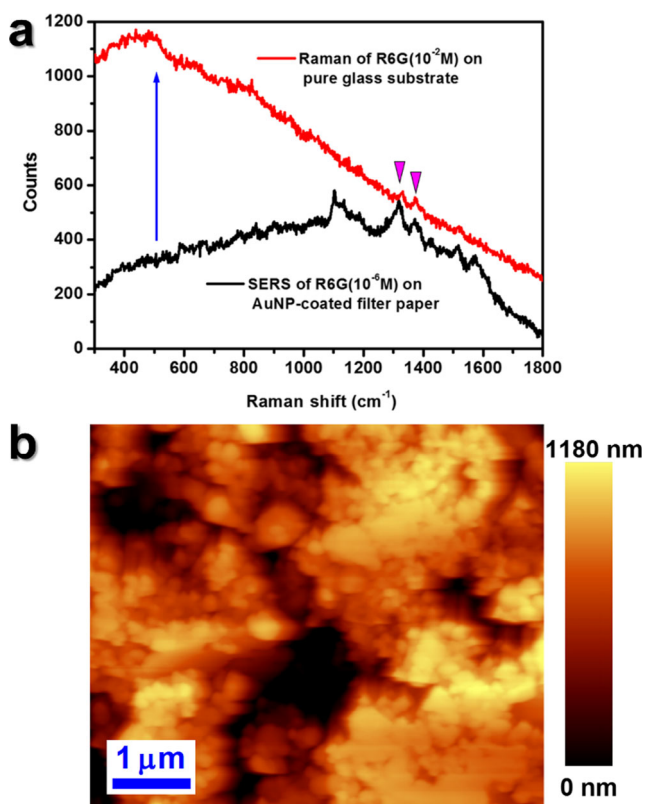


Fig. 6 (a) SERS spectrum (black) measured on R6G molecules prepared by drop casting R6G/ethanol solution with a concentration of 10^{-6} M onto an AuNP-coated filter paper substrate and Raman spectrum (red) measured on the sample prepared by drop-casting R6G/ethanol solution with a concentration of 10^{-2} M onto the surface of a piece of glass. (b) Atomic force microscopic (AFM) image measured on the SERS substrate using filter papers

hotspots, and enlarged total interaction area with improved contacts.

As has been investigated [38], the surface roughness not only induces direct reflection or scattering, which may be assigned as first-order processes for enhancing local fields, but also produces secondary interactions. Wave vector conservation rules have to be satisfied, where incident wave vector is modified by $K_g = K_i + g$ in the transmission and reflection waves with K_i and g defined as the wave vector of incidence and the g th spatial Fourier component of the reciprocal lattice wave vector, respectively. Detailed discussions and investigations can be found in [38]. The rough surfaces produced by the combination between the AuNPs and paper fibers supplied additional enhancement mechanisms for the SERS performance. We report a paper-based SERS substrate, where TOABr-coated gold nanoparticles are supported by a 3D network of paper fibers. Three types of papers that are commonly available are employed to prepare the substrates. However, filter papers are found to be a best choice for the design of the most stable 3D plasmonic structures, where SERS signals with high enhancement factor and high signal-to-noise ratio are achieved. Enhancement factors larger than 10^4 have been

measured in the detection of R6G molecules by drop-casting low concentration solutions onto the paper-based SERS substrates. The presented method not only introduces a simple, low-cost, and conveniently achievable approach for the SERS detection but also demonstrates important mechanisms for high-sensitivity sensing techniques. In particular, paper-based substrate implies easily tailorable into expected shapes and sizes of the SERS substrates. Furthermore, the flexible paper-based SERS devices are apparently disposable and environment friendly.

Materials and Methods

Chemicals and Materials

Sodium borohydride (NaBH_4 , 99%), tetraoctylammonium bromide ($\text{C}_{32}\text{H}_{68}\text{BrN}$, 99%), methanol, toluene (C_7H_8 , 99.9%), and tetrachloroauric acid ($\text{HAuCl}_4 \cdot 4\text{H}_2\text{O}$) were purchased from Aldrich Chemical. Deionized water purified by Thermo scientific D50282 ($17.8 \text{ M}\Omega \cdot \text{cm}$) was employed for all aqueous solutions.

Synthesis of Tetraoctylammonium Bromide (TOABr)-Coated AuNPs

TOABr-coated AuNPs were synthesized by Brust method without addition of thiol reagents. Tetraoctylammonium bromide (1.5 g/2.74 mmol) is dissolved into 80 mL toluene in a double-mouth round bottom flask; then, $\text{HAuCl}_4 \cdot 4\text{H}_2\text{O}$ (0.44 mmol) dissolved in 2 mL deionized water is added. After 20 min of reaction, NaBH_4 (0.28 g) in 20 mL deionized water was quickly poured into the reaction vessel. The reaction mixture is rapidly stirred at room temperature for 5 min. The organic phase is reserved and the solvent is removed below 50°C on a rotary evaporator. The product was then aggregated in methanol. After being dried in vacuum, the TOABr-coated AuNPs were obtained. In the last stage, the TOABr-coated AuNPs were suspended in acetone with different concentrations for later use.

Preparation of the Paper Substrates

Porosity is necessary for the AuNPs to be adsorbed onto the fibers of the papers. 3D arrangement of the paper fibers allows the enlargement of the total surface area for better contacting of the molecules with the gold nanoparticles. Filter papers, printing papers, and envelope papers were cut into pieces with the same square shape and an equal area of 100 mm^2 , which were used as the substrates for further metallization.

Fabrication of the Paper-Based SERS Substrates

A 30 μL TOABr-AuNPs in acetone with a concentration of 50 mg/mL were drop-cast onto the paper substrates. These samples were then placed on a hotplate and heated at 110°C for 90 s. After complete evaporation of acetone, TOABr-AuNPs were firmly adsorbed onto the surface of papers.

Morphology Characterization

Scanning electron microscopic (SEM) images were acquired by a JEOL JSM-6700F at a voltage of 15 kV and an electron current of 92 μA . Fluorescence optical microscopic images were obtained by an Olympus microscope BX51.

SERS Performance Characterization

A 785 nm laser with an output power of 100 mW and a linewidth of 0.72 nm was used as the excitation light source. A Raman spectrometer from Ocean Optics (QEP01609) has an effective spectral range of 2098 cm^{-1} and a resolution of 0.16 nm. All the Raman spectra were acquired with an integration time of 1 s.

Acknowledgements The authors acknowledge the National Natural Science Foundation of China (NSFC) (61735002, 11574015, 11434016) and the Beijing Key Lab of Microstructure and Property of Advanced Materials for the support.

References

- Li M, Paidi SK, Sakowski E, Preheim S, Barman I (2019) Ultrasensitive detection of hepatotoxic microcystin production from cyanobacteria using surface-enhanced Raman scattering immunosensor. *ACS Sensors* 4:1203–1210
- Chang S, Yun W, Eichmann SL, Poitzsch ME, Wang W (2019) Magnetic SERS composite nanoparticles for microfluidic oil reservoir tracer detection and nanoprobe applications. *ACS Appl NanoMater* 2:997–1004
- Wang C, Wang C, Wang X, Wang K, Zhu Y, Rong Z, Wang W, Xiao R, Wang S (2019) Magnetic SERS strip for sensitive and simultaneous detection of respiratory viruses. *ACS Appl Mater Interfaces* 11:19495–19505
- Fu G, Sun D, Pu H, Wei Q (2019) Fabrication of gold nanorods for SERS detection of thiabendazole in apple. *Talanta* 195:841–849
- Sitjar J, Liao J, Lee H, Liu BH, Fu W (2019) SERS-active substrate with collective amplification design for trace analysis of pesticides. *Nanomaterials* 9:664–612
- Kang Y, Wu T, Chen W, Li L, Du Y (2019) A novel metastable state nanoparticle-enhanced Raman spectroscopy coupled with thin layer chromatography for determination of multiple pesticides. *Food Chem* 270:494–501
- Tian L, Su M, Yu F, Xu Y, Li X, Li L, Liu H, Tan W (2018) Liquid-state quantitative SERS analyzer on self-ordered metal liquid-like plasmonic arrays. *Nat Commun* 9:3642–3612
- Wu H, Luo Y, Hou C, Huo D, Zhou Y, Zou S, Zhao J, Lei Y (2019) Flexible bipyramid-AuNPs based SERS tape sensing strategy for detecting methyl parathion on vegetable and fruit surface. *Sensors Actuators B Chem* 285:123–128
- Li X, Yang T, Song Y, Zhu J, Wang D, Li W (2019) Surface-enhanced Raman spectroscopy (SERS)-based immunochromatographic assay (ICA) for the simultaneous detection of two pyrethroid pesticides. *Sensors Actuators B Chem* 283:230–238
- Wang H, Yang K, Hsu S, Huang MH (2016) Photothermal effects from au-Cu₂O core-shell nanocubes, octahedra, and nanobars with broad near-infrared absorption tunability. *Nanoscale* 8:965–972
- Joseph D, Baskaran R, Yang SG, Huh YS, Han Y (2019) Multifunctional spiky branched gold-silver nanostars with near-infrared and short-wavelength infrared localized surface plasmon resonances. *J Colloid Interface Sci* 542:308–316
- Atta S, Celik FE, Fabris L (2019) Enhancing hot electron generation and injection in the near infrared via rational design and controlled synthesis of TiO₂-gold nanostructures. *Faraday Discuss* 214:341–351
- Wei Y, Zhang X, Liu Z, Chen H, Yang P (2019) Site-selective modification of AgPt on multibranching Au nanostars for plasmon-enhanced hydrogen evolution and methanol oxidation reaction in visible to near-infrared region. *J Power Sources* 425:17–26
- Miscuglio M, Borys NJ, Spirito D, Martín-García B, Zaccaria RP, Weber-Bargioni A, Schuck PJ, Krahn R (2019) Planar aperiodic arrays as metasurfaces for optical near-field patterning. *ACS Nano* 13:5646–5654
- Li X, Iqbal MA, Xu M, Wang Y, Wang H, Jie M, Wan X, Slater TJA, Liu J, Liu J, Rong H, Chen W, Kershaw SV, Haig SJ, Rogach AL, Xie L, Zhang J (2019) Au@Hg_xCd_{1-x}Te core@shell nanorods by sequential aqueous cation exchange for near-infrared photodetectors. *Nano Energy* 57:57–65
- Huang Z, Meng G, Hu X, Pan Q, Huo D, Zhou H, Ke Y, Wu N (2019) Plasmon-tunable Au@Ag core-shell spiky nanoparticles for surface-enhanced Raman scattering. *Nano Res* 12:449–455
- Liu Z (2017) One-step fabrication of crystalline metal nanostructures by direct nanoimprinting below melting temperatures. *Nat Commun* 8:14910–14917
- de Aberasturi DJ, Serrano-Montes AB, Langer J, Henriksen-Lacey M, Parak WJ, Liz-Marzán LM (2016) Surface enhanced Raman scattering encoded gold nanostars for multiplexed cell discrimination. *Chem Mater* 28:6779–6790
- Leonardi A, Engel M (2018) Particle shape control via etching of core@shell nanocrystals. *ACS Nano* 12:9186–9195
- Mahmoud KA, Zourob M (2013) Fe₃O₄/Au nanoparticles/lignin modified microspheres as effectual surface enhanced Raman scattering (SERS) substrates for highly selective and sensitive detection of 2,4,6-trinitrotoluene (TNT)†. *Analyst* 138:2712–2719
- Ling X, Xie L, Fang Y, Xu H, Zhang H, Kong J, Dresselhaus MS, Zhang J, Liu Z (2010) Can Graphene be used as a substrate for Raman enhancement? *Nano Lett* 10:553–561
- Cong S, Wang Z, Gong W, Chen Z, Lu W, Lombardi JR, Zhao Z (2019) Electrochromic semiconductors as colorimetric SERS substrates with high reproducibility and renewability. *Nat Commun* 10:678–610
- Zhang D, You H, Yuan L, Hao R, Li T, Fang J (2019) Hydrophobic slippery surface-based surface-enhanced Raman spectroscopy platform for ultrasensitive detection in food safety applications. *Anal Chem* 91:4687–4695
- Morales-Narváez E, Merkoçi A (2019) Graphene oxide as an optical biosensing platform: a progress report. *Adv Mater* 31:1805043–1805012
- Kanipe KN, Chidester PPF, Stucky GD, Moskovits M (2016) Large format surface-enhanced Raman spectroscopy substrate optimized for enhancement and uniformity. *ACS Nano* 10:7566–7571

26. Liao W, Lin Q, Xu Y, Yang E, Duan Y (2019) Preparation of Au@Ag core-shell nanoparticle decorated silicon nanowires for bacterial capture and sensing combined with laser induced breakdown spectroscopy and surface-enhanced Raman spectroscopy. *Nanoscale* 11:5346–5354
27. Mitsai E, Kuchmizhak A, Pustovalov E, Sergeev A, Mironenko A, Bratskaya S, Linklater DP, Balčytis A, Ivanova E, Juodkazis S (2018) Chemically non-perturbing SERS detection of a catalytic reaction with black silicon. *Nanoscale* 10:9780–9787
28. Lee Y, Kamal ASA, Abasaki M, Ho Y, Takakura Y (2016) Gap plasmons multiple mirroring from spheres in pyramids for surface-enhanced Raman scattering. *ACS Photonics* 3:2405–2412
29. Singh N, Prakash J, Misra M, Sharma A, Gupta RK (2017) Dual functional ta-doped electrospun TiO₂ nanofibers with enhanced photocatalysis and SERS detection for organic compounds. *ACS Appl Mater Interfaces* 9:28495–28507
30. Xiong R, Kim HS, Zhang S, Kim S, Korolovych VF, Ma R, Yingling YG, Lu C, Tsukruk VV (2017) Template-guided assembly of silk fibroin on cellulose nanofibers for robust nanostructures with ultrafast water transport. *ACS Nano* 11:12008–12019
31. Song W, Ji W, Vantasin S, Tanabe I, Zhao B, Ozaki Y (2015) Fabrication of a highly sensitive surface-enhanced Raman scattering substrate for monitoring the catalytic degradation of organic pollutants. *J Mater Chem A* 3:13556–13562
32. Wu H, Sun X, Hou C, Hou J, Lei Y (2018) Preparation of quasi-three-dimensional porous Ag and Ag-NiO nanofibrous mats for SERS application. *Sensors* 18:2862–2811
33. Yang Y, Zhang Z, He Y, Wang Z, Zhao Y, Sun L (2018) Fabrication of Ag@TiO₂ electrospinning nanofibrous felts as SERS substrate for direct and sensitive bacterial detection. *Sensors Actuators B Chem* 273:600–609
34. Kwon G, Kim J, Kim D, Ko Y, Yamauchi Y, You J (2019) Nanoporous cellulose paper-based SERS platform for multiplex detection of hazardous pesticides. *Cellulose* 26:4935–4944
35. Liu Z, Yan Z, Jia L, Song P, Mei L, Bai L (2017) Liu Y. Gold nanoparticle decorated electrospun nanofibers: a 3D reproducible and sensitive SERS substrate. *Appl Surf Sci* 403:29–34
36. Rao VK, Radhakrishnan TP (2015) Tuning the SERS response with Ag-au nanoparticle-embedded polymer thin film substrates. *ACS Appl Mater Interfaces* 7:12767–12773
37. Mei H, Zhao X, Bai S, Li Q, Xia J, Bai H, Cheng L (2018) Tuning SERS properties of pattern-based MWNTs-AuNPs substrates by adjustment of the pattern spacings. *Carbon* 136:38–45
38. Moskovits M (1985) Surface-enhanced spectroscopy. *Rev Mod Phys* 57:783–826

Publisher's Note Springer Nature remains neutral with regard to jurisdictional claims in published maps and institutional affiliations.